

Use of Geomatic Techniques for Mapping Suspended Solids in Aquatic Ecosystems: The Case Study of Guayas River, Ecuador

Jennyffer Rebeca Yopez Ramírez

Facultad de Ciencias e Ingeniería, Universidad Estatal de Milagro, Milagro, Ecuador
jyopezr5@unemi.edu.ec (corresponding author)

Rayner Reinaldo Ricaurte Parraga

Facultad de Ciencias e Ingeniería, Universidad Estatal de Milagro, Milagro, Ecuador
rricaurtep@unemi.edu.ec

Jesus Armando Verdugo Arcos

Facultad de Ciencias e Ingeniería, Universidad Estatal de Milagro, Milagro, Ecuador
jverdugoal@unemi.edu.ec

Received: 7 August 2024 | Revised: 30 August 2024 | Accepted: 4 September 2024

Licensed under a CC-BY 4.0 license | Copyright (c) by the authors | DOI: <https://doi.org/10.48084/etasr.8664>

ABSTRACT

Satellite images cover large remote areas and are useful for detecting and monitoring water bodies. In Ecuador, since 1950, the lower Guayas River basin has undergone significant natural and anthropogenic changes that have impacted its dynamics and sustainability. This study aims to analyze through in situ data and geomatic techniques the change that the river has undergone in a decade by mapping the Suspended Sediment Concentration (SSC). Increasing levels of pollution in the river have raised concerns, prompting various approaches to measure and mitigate sedimentation to maintain the sustainable quality of the watershed. The spatiotemporal variations of SSC in the Guayas River revealed a remarkable variability, influenced by the operation of reservoirs, changes in land use, erosion, and sedimentation causing SSC in 2013 to range from 64.82 to 707.06 mg/l in the satellite image of 9/16/2013 and from 87.58 to 933.36 mg/l in the image of 7/26/2023. Understanding this distribution is crucial for the environmental protection and sustainability of aquatic ecosystems. This study used Landsat 8 data, an atmospheric pre-correction, and a remote sensing model. The results indicate a creasing trend of SSC in the stretches of the Guayas River between 2013 and 2023, which allows the understanding of the spatiotemporal dynamics of suspended sediment transport.

Keywords-geomatic techniques; Suspended Sediment Concentration (SSC); Landsat; Guayas River; satellite; atmospheric correction

I. INTRODUCTION

Water resource management, in terms of quality, distribution, and quantity, is one of the most important tasks that has significantly contributed to the progress of the economic and social welfare of the regions during the last decade [1]. Climate change represents one of the greatest threats to the planet and poses a significant challenge to the sustainable management of water resources [2, 3]. Increased erosion, sediment transport, and their accumulation indicate the adaptation of natural river systems to the new climatic conditions in the area [4]. South America contributes more freshwater runoff to the ocean per square kilometer of land area than any other continent, while much of this water enters the river system from the headwaters of the Andes Mountains [5]. In Ecuador, the mountain range crosses the territory from the

north to south and contains different types of soil. Important spatial and temporal fluctuations in the vegetation cover are frequently associated with significant changes in the land use and topographic configuration, as well as with a great variety of climatic zones, and the greatest biodiversity in the world per unit area in a territory of only 256,370 km² [6–8].

The Guayas River basin, which belongs to the Guayas hydrographic system, is the largest in Ecuador and one of the most important river systems in the country [9]. The area is presently experiencing significant socioeconomic and environmental challenges stemming from the morphodynamic evolution of rivers and estuaries. These issues arise from the interplay between hydrodynamic conditions, channel geometry, and sediment availability [10–13]; this is the result of anthropogenic actions, such as mangrove deforestation,

inadequate watershed management [14], overexploitation of natural resources, inadequate construction of infrastructure works without prior feasibility studies, and changes in land use [15], which in combination with human activity often leads to deterioration of the quality of the available water [16].

Soil erosion is a natural process that degrades soil [17] and is defined as the network of all long-term processes that detach soil and move it from its original position [18]. Water erosion is a type of erosion that affects more the land surface. The detachment of soil occurs in two ways: by the splashing of the raindrops on the soil surface and by the forces exerted by water flowing across the surface, known as runoff [19].

Total Suspended Solids (TSS) are composed of organic and inorganic materials that are introduced into water bodies through runoff, dredging activities in coastal waters, and resuspension events, in the form of sediment [20,21]. Suspended sediments are optically active constituents that can decrease the light penetration through the water column [22-24]. The Suspended Sediment Concentration (SSC) plays a crucial role in regulating the available light in aquatic ecosystems, and significantly influences the development of aquatic plants and algae.

Accurate knowledge of the processes occurring in river basins makes it possible to monitor changes and track modifications in the environmental, ecological, and social settings of water bodies. The traditional method employed for the study of watersheds focuses on field sampling, which involves on-site surveying and data acquisition and presents challenges such as high labor costs and the need for more rigorous statistical accuracy. In addition, fieldwork carries risks to personnel safety. Over time, remote sensing technology has undergone continuous evolution, with platform upgrades and the progressive emergence of new sensors. The introduction of Earth Observation (EO) systems has marked a significant change in the way individuals understand and analyze the terrestrial landscape. The availability of satellite imagery, including Hyper-Spectral Imaging (HSI), Multi-Spectral Imaging (MSI), Synthetic-Aperture Radar (SAR), and Light Detection and Ranging (LiDAR), has enabled the detailed analysis of land surfaces and water bodies [25]. With the emergence of free satellite data, water body data extraction processes have evolved significantly, taking advantage of the latest innovations in remote sensing satellites such as NASA's Landsat and Sentinel-2 launched by ESA.

II. STUDY AREA

The Guayas River basin, situated in the central-western region of Ecuador, spans from 0° S to 3° S latitude and from 81° W to 78° W longitude. Renowned for its vast size, high agricultural productivity, and substantial economic contributions, it is one of Ecuador's principal basins. Covering an area of 33,700 km², the basin receives an average annual rainfall of 1,662 mm and has an average annual flow of 974 m³/s, eventually discharged into the Gulf of Guayaquil [26]. The basin is bordered to the north by the Esmeraldas hydrographic district; to the south by the Jubones and Santiago districts; to the east by the Pastaza and Santiago hydrographic

districts; and to the west by the Manabí district and the Pacific Ocean.

It corresponds to 13% of the Ecuadorian territory, and it concentrates about 40% of the country's total population. The rainy season lasts from September to May, a period in which the 70% to 95% of precipitation occurs. Average annual precipitation varies according to the geographic direction, decreasing from north to south and from east to west. It starts at 3,000 mm in the northeastern limit, in Santo Domingo de los Colorados, decreasing to 2,200 mm in Quevedo, to 1,200 mm in the areas near the cities of Babahoyo and Daule, to 1,000 mm in Guayaquil, and to 750 mm in Chongón in the extreme southwest [9].

The Guayas River is the main source of fresh water in the region. Currently, the main environmental challenges facing the freshwater ecosystems are pollution from sewage and agriculture, changes in land use, and the presence of two hydroelectric dams located in the upper part of the basin [27]. The Palmar islet (Figure 1), situated at the junction of the Daule and Babahoyo rivers, is considered the most notable and conspicuous manifestation of sedimentation in the Guayas River. Its expansion induces erosion along the adjacent banks and attracts birds, which hinders the takeoff and landing of aircraft at the nearby Guayaquil International Airport.

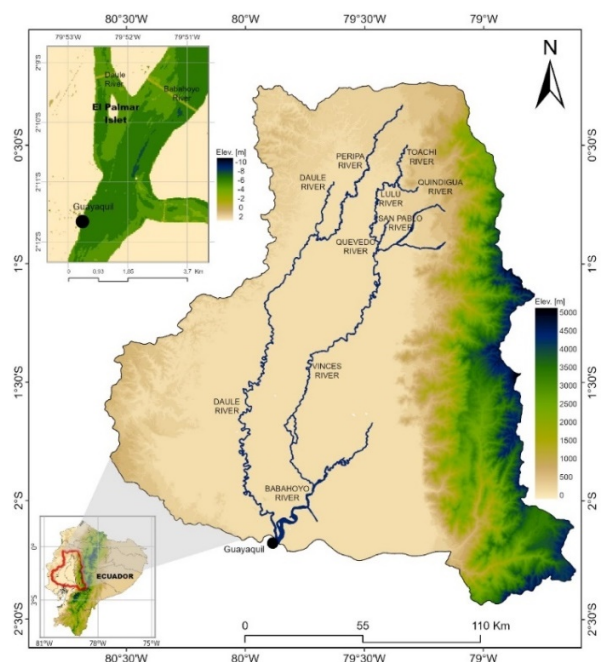


Fig. 1. El Palmar islet.

III. DATA COLLECTION

A total of 10 satellite images were acquired from satellite Landsat 8, in the span between September 16, 2013 and July 26, 2023, to assess the impact of sediment accumulation over a 10 year period. The specifics of these images, including the capture time, solar geometry, path/row, and environmental conditions at the time of acquisition, are provided in Table I.

TABLE I. AREA IMAGES FROM SATELLITE LANDSAT 8

No.	ID Level	Path/Row	Capture Date	Sun Elevation/Azimuth	Sky Coverage
1	LC80110612013259LGN01	127/45	2013/09/16	64.406/81.367	28.28
2	LC80110622014358LGN01	127/45	2014/12/24	56.646/ 130.293	26.06
3	LC80110622015313LGN01	127/45	2015/11/09	63.223/ 123.048	14.76
4	LC80110622016364LGN01	127/45	2016/12/29	56.276/129.341	21.50
5	LC80110622017350LGN00	127/45	2017/12/16	57.417/131.106	24.12
6	LC80110622018097LGN00	127/45	2018/04/07	60.379/70.448	27.20
7	LC80110622019148LGN00	127/45	2019/05/28	54.249/45.752	29.79
8	LC80110622021137LGN00	127/45	2021/05/17	55.639/48.289	26.73
9	LC80110622022364LGN00	127/45	2022/12/30	56.284/129.283	28.28
10	LC80110622023207LGN00	127/45	2023/07/26	53.801/50.802	28.43

The Guayas Hydrological District is equipped with seventeen hydrological stations for strategic monitoring. Due to the insufficient availability of hydrological monitoring data provided by the competent regulatory entity in Ecuador, this study chooses to focus on the use of data acquired through geomatics techniques. These techniques allow the collection of remote and continuous information, offering a viable and effective alternative to the limitations found in conventional monitoring methods. This approach not only ensures extensive coverage of the study area, but also allows for a more dynamic and up-to-date assessment of hydrological conditions.

Collecting data on SSC in the field requires a significant investment of time and financial resources. The evaluation of time series using on-site measurements is constrained by factors, such as the number of sampling points, the frequency of monitoring, and the geographic scope available. In some cases, data may not be available for certain periods of time. Therefore, it is essential to resort to satellite remote sensing information, which provides extensive spatial coverage and continuous records over time, to monitor spatiotemporal fluctuations in the concentration of suspended solids in coastal areas. Satellites are indispensable for monitoring water quality over large and often inaccessible areas. These optical instruments usually are in heliosynchronous orbits, except for GOCI which is in geostationary orbit for the observation of specific water bodies, and provides spatial coverage ranging from tens to hundreds of kilometers [28, 29]. The periodicity of observation of these devices varies from one-hour to one-week intervals, which allows constant monitoring of the water bodies.

Numerous studies have demonstrated the effectiveness of Landsat data for monitoring river turbidity and SSC. These data have a spatial resolution of 30 meters and provide access to long time records going back to 1984, which facilitates long-term monitoring [30]. Therefore, to carry out this analysis, it has been decided to use data obtained from the Operational Land Imager on board Landsat 8-9 (OLI/Landsat 8-9) satellites. The choice of this specific dataset aims to examine the SSC in the lower Guayas River basin reach during a 10-year study period spanning from 2013 to 2023. Two main features of Landsat-8 data are the high resolution and reliability, which render them suitable for observing and quantifying temporal and spatial changes in river water quality during the specified interval.

IV. THE PROPOSED APPROACH

The atmospheric correction (removing the scattering and absorption effects of the atmosphere of the images) for the study area is carried out using the Landsat 8-9 Operational Land Imager (OLI) - Thermal Infrared Sensor (TIRS) Collection 2 Level 1 (L1) product with ERDAS IMAGINE 2022 software. The image dataset includes bands 1 to 7 with data type UINT16. To achieve the atmospheric correction, it is first needed to convert the initial Digital Numbers (DN) of the satellite images to Top-Of-Atmosphere (TOA) radiance $L_{TOA}(\lambda)$ ($W \cdot m^{-2} \cdot sr^{-1} \cdot \mu m^{-1}$) by using (1) and then convert $L_{TOA}(\lambda)$ to the unitless TOA reflectance $\rho_{TOA}(\lambda)$ by utilizing (2) [31];

$$L_{TOA}(\lambda) = \alpha_{\lambda} \cdot DN + \beta_{\lambda} \quad (1)$$

where λ indicates the band and α_{λ} and β_{λ} are band-specific rescaling factors;

$$\rho_{TOA}(\lambda) = \frac{\pi \cdot L_{TOA}(\lambda)}{E_0(\lambda) \cdot \cos \theta} \quad (2)$$

where $E_0(\lambda)$ ($W \cdot m^{-2} \cdot sr^{-1} \cdot \mu m^{-1}$) and θ ($^{\circ}$) are the solar spectral irradiance and the sun zenith angle, respectively.

This study primarily utilized the following bands: blue (B), green (G), red (R), near infrared (NIR), and shortwave infrared (SWIR).

In this analysis, the ERDAS IMAGINE software platform was deployed, as it is an essential tool for working with data from remote sensing and spatial analysis. Also MATLAB was used for analyses, such as linear regression, visualization of scatter diagrams, and significance tests. In addition, ArcGIS Pro 3.2.0 software was employed to create maps with precise geo-graphic references, which facilitates the visualization and spatial interpretation of the data.

In water bodies the reflectance calculated by geomatic techniques is determined by considering the properties and characteristics of the optically active substances. The reflectance is exponentially decreasing from the blue band to the red band for water, in its natural state. The reflectance curve changes when different substances, such as sediments, are present in the water. This results in water bodies with various concentrations of suspended sediments, which will exhibit variations in their inherent optical properties, particularly regarding light absorption and scattering. Consequently, the reflectance spectra of these water bodies

change according to the different SSC. In normal conditions, reflectance shows an increase in the red-green band as the SSC increases. With increasing SSC, the peak reflectance in this band tends to saturate and shift toward longer wavelengths, a phenomenon known as "redshift" [32].

There are different models that calculate the SSC in the water bodies. Table II presents the models for Ganges and Brahmaputra, middle-upper Changjiang river, and river Guayas.

TABLE II. MODELS FOR CALCULATING THE SSC

Study Region (SSC, mg/L)	Sensor / Satellite	Formulas	Factor		R ²
			a ₀	a ₁	
Ganges and Brahmaputra (0-1200)	TM / Landsat-5	SSC = a ₀ + a ₁ × G	-14,997	100,026	0.20
Middle-upper Changjiang River (22.0-2610)	ETM+ / Landsat-7	ln (SSC) = a ₀ + a ₁ × ln (NIR)	12.72	2.90	0.68
River Guayas (64.82-933.36)	OLI / Landsat-8	SSC = a ₀ × exp (a ₁ × (G+R)/(G/R))	3.501	4.317	0.79

This study utilizes the model for the Guayas River considering the Green (G) and Red (R) bands on the data from the OLI sensor on the Landsat-8 satellite. The model is defined by:

$$SSC = a_0 \cdot \exp \left[a_1 \cdot \frac{G+R}{\frac{G}{R}} \right] \tag{3}$$

where G and R represent the spectral bands, a₀ is the intercept or base coefficient, which acts as the initial scaling factor, and a₁ modulates the exponent and reflects how the relationship between the green and red bands affects the calculated SSC. The values of a₀ and a₁ for the case of Guayas River are 3.501 and 4.317, respectively.

To evaluate the quality of the fit of the model, different images corresponding to the Landsat series were selected, with less than 30% cloud cover, which improves the quality of the data used in the modeling. Subsequently, the remotely sensed data were compared with daily SSC data from the hydrological stations. A total of 60 pairs of high-quality data were obtained. Out of these, 75% (45 pairs) were randomly selected for model development, while the remaining 25% (15 pairs) were used for model validation.

For this evaluation the coefficient of determination (R²) was calculated ensuring a level of statistical significance with a value of p < 0.01 in a two-tailed test and its value is 0.79 (Table II), which indicates the model's ability to explain the variability in the SSC measurements as a function of measured reflectance. To verify the accuracy of the SSC determined by remote methods, statistical measures, such as Mean Absolute Percent Difference (MAPD) (%) (4), Root Mean Square Error (RMSE) (mg/L) (5), and Relative Bias (RB) (%) (6) were applied. These metrics were calculated utilizing specific formulas that allow to quantify the errors and accuracy of the SSC values derived from the analyzed images, providing a robust assessment of the model's ability to replicate and predict the real conditions observed in the field:

$$MAPD = \left\{ \frac{[X_i^{modeled} - X_i^{in-situ}]}{X_i^{in-situ}} \right\} \cdot \frac{100}{N} \tag{4}$$

$$RMSE = \left\{ \frac{[X_i^{modeled} - X_i^{in-situ}]^2}{N} \right\}^{\frac{1}{2}} \tag{5}$$

$$RB = \left\{ \frac{\frac{1}{N} \cdot \sum [X_i^{modeled} - X_i^{in-situ}]}{mean(X_i^{in-situ})} \right\} \cdot 100 \tag{6}$$

where X_i^{modeled}, X_i^{in-situ} are the SSC calculated by the model and the SSC measured directly in the field, respectively and N the total number of samples collected.

To examine the temporal variability and spatial distribution of SSC in the lower Guayas River, the coefficient of variation CV, as defined by (7), was used:

$$CV = \frac{\sqrt{\frac{1}{N} \cdot \sum (SSC_i - \overline{SSC})^2}}{\overline{SSC}} \tag{7}$$

where SSC_i is the annual SSC for each year, \overline{SSC} is the mean of all SSC_i's, and N is the total number of the years analyzed, which in this case is 10 years.

This statistical indicator allows for evaluating the dispersion of the SSCs around the mean during a significant period, covering the ten years between 2013 and 2023. The CV is valuable here, as it reveals the spatial heterogeneity of SSC, pointing out areas with notable changes that may indicate environmental impacts, sediment transport dynamics or human effects on the river. This analysis contributes to understanding the complex interactions and variability of suspended sediments, which improves river ecosystem management and conservation strategies.

V. RESULTS AND DISCUSSION

Landsat-8 spectral reflectance shows variations according to SSC levels. Figures 2 and 3 present the ρ_{TOA} curves with varying SSC's for two days; 9/16/2013 (Figure 2) and 7/26/2023 (Figure 3). The colored rectangles in both figures indicate the ranges of the five spectral bands (B: blue, G: green, R: red, NIR: near-infrared, and SWIR: short-wave infrared). The values that are observed varied from 87.58 to 933.36 mg/L on 9/16/2013 and from 64.82 to 707.06 mg/L on 7/26/2023.

When the concentration of SSC is low, the ρ_{TOA} across all five spectral bands is similarly low, with the highest reflectance observed in the green band. As the suspended SSC increases, the reflectance in the first four bands displays a significant increase, whereas in the shortwave infrared (SWIR) band the changes are more variable, with most of the reflectance peaks being observed in the near infrared band (NIR).

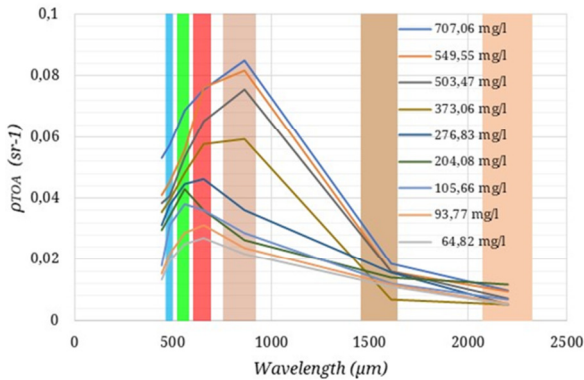


Fig. 2. Spectral curves of waters according to SSC for 9/16/2013.

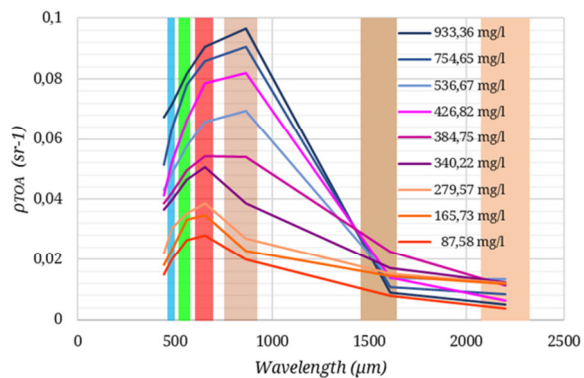


Fig. 3. Spectral curves of waters according to SSC for 7/26/2023.

Figures 4 and 5 portray the values of SSC obtained by the model and the correlation between SSC and remote-sensing reflectance (Rrs) for 2013 and 2023, respectively.

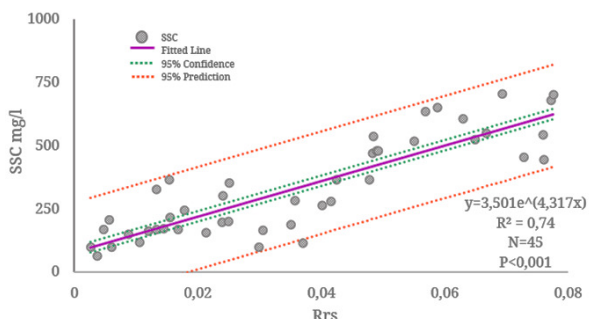


Fig. 4. SSC and remote-sensing reflectance for 2013.

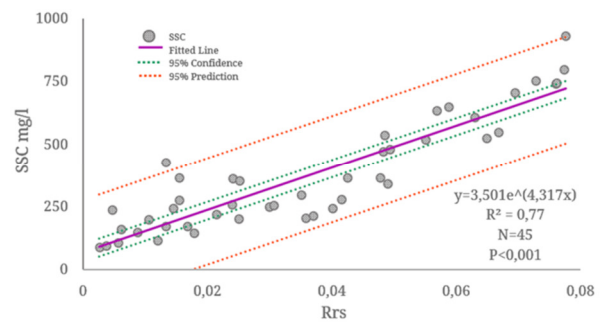


Fig. 5. SSC and remote-sensing reflectance for 2023.

From the validation of the model it emerged that it is applicable for remotely estimating CSS using Landsat 8 data. As illustrated in Figures 6 and 7, all data points, both for 2013 and 2023, were distributed along the 1:1 line for the years evaluated, indicating good accuracy in estimating high and low levels of SSC in the Lower Basin of the Guayas River-Islet El Palmar. The MAPD was 32.93% in 2013 and 23.85% in 2023 for the development dataset, with an RMSE of 85.81 mg/L in 2013 and 82.95 mg/L in 2023, and an RB of -25.87% in 2013 and -22.87% in 2023. For the evaluation dataset, the MAPD was 33.57% in 2013 and 31.48% in 2023, with an RMSE of 84.73 mg/L in 2013 and 82.06 mg/L in 2023, and an RB of -26.04% in 2013 and -23.37% in 2023. The difference is not considered significant between the field-derived data and the Landsat 8 data, which means that there is a constant trend of change between the Landsat 8 derived SSC and the hydrological monitoring data.

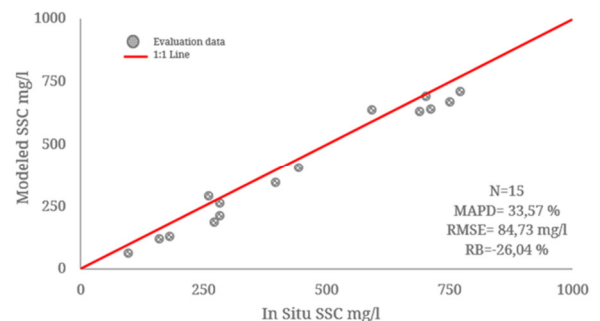


Fig. 6. In situ SSC and model SSC comparison for 2013.

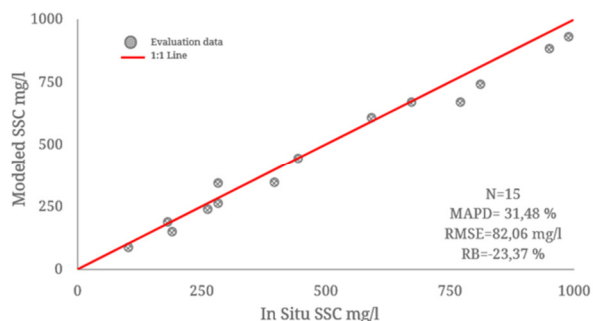


Fig. 7. In situ SSC and model SSC comparison for 2023.

Atmospheric corrections are essential to obtain accurate measurements of sediments in water bodies through geomatics techniques. These corrections eliminate atmospheric influences, such as scattering and absorption of solar radiation, which can distort signals reflected from the surface of water bodies. Applying these corrections increases the accuracy of SSC estimates and ensures the temporal and spatial consistency of the data. This allows comparison of satellite images captured at different times and locations, facilitating long-term monitoring and trend analysis. Atmospheric corrections are also essential for the calibration and validation of remote sensing models, ensuring that decisions based on these data are accurate and reliable. With the atmospheric corrections of the Landsat 8 images by using (2) and then the model of (3) for processing, the SSC could be obtained. The average SSC of several years presents the significant spatial pattern of being high in the lower Guayas River-Islet El Palmar basin, with the highest concentration in 2023, due to the large number of sediments that are deposited from the estuaries of the Babahoyo and Daule rivers.

The application of model (3) to Landsat data allowed the determination of the SSC in the lower Guayas River-Islet El Palmar basin from 2013 to 2023. The arithmetic mean value was then calculated to obtain the climatological SSC. The spatial distribution of the climatological CSS and its CV indicated that the construction of the Daule-Peripa river reservoir has caused an essential impact on sediment transport in the Guayas River, with the sediments being deposited in the lowest part of the river body. Furthermore, anthropogenic activities significantly contribute to the increase in sediment load. Deforestation, particularly in the upper and middle zones of the watershed, has exposed large tracts of soil to erosion, thus increasing the amount of sediment carried by runoff into the river. Intensive agricultural practices, such as excessive use of fertilizers and pesticides, have exacerbated this problem by stripping the soil of its protective layer and increasing its vulnerability to erosion. On top of this, the impact of urbanization and the expansion of infrastructure have altered the natural landscape, increasing surface runoff and soil erosion.

Water flow is a determining factor affecting sediment transport in the lower reaches of the Guayas River. During periods of high flow, sediments are entrained and resuspended, increasing the SSC. In contrast, when flow is low, sediment tends to settle and accumulate, resulting in a decrease in SSC. This is the case of El Palmar islet, whose appearance was due to sedimentation and accumulation of suspended sediments due to relatively low flows [33].

VI. CONCLUSIONS

Sedimentation and anthropogenic activities have an adverse impact on the sustainability of the lower Guayas River basin. An illustrative example is the appearance of the El Palmar islet, whose emergence is attributed to natural processes of sedimentation and erosion that have been developed over time. The literature reviewed indicates that geomatic techniques offer a comprehensive system for the monitoring of several of the main pollutants that affect the river systems. Currently, the monitoring of water bodies is carried out using a variety of

satellite sensors, such as AVHRR, GOCI, Landsat, MODIS, OLCI, Sentinel-2 and VIIRS, which provide spectral and spatial resolutions capable of detecting contaminants and other parameters hydric.

This study evaluated the variations of suspended solids concentration (SSC) using geomatics techniques during the last decade. A remote sensing model was applied to the Landsat data to observe SSC in the lower Guayas River basin, with an MADP of 33.57% and RMSE of 84.73 mg/L in 2013, and an MADP of 31.48% and RMSE of 82.06 mg/L in 2023. It has been shown that the data obtained from satellite images allow for effectively mapping the distribution of SSC in the lower Guayas River basin, El Palmar Islet. The results indicate that the SSC in the evaluated area has undergone changes in both its spatial and temporal distribution.

The spatial distribution of SSC in the lower Guayas River basin has exhibited a pronounced upward trend over the past decade, with noticeable increases observed in most areas of the river. This phenomenon warrants further investigation for its implications to be understood. There is an urgent need to tackle the rising levels of SSC in relation to estuarine management, coastal protection, and the broader economic, environmental, and social dimensions of sustainability. The increased sediment production from the Guayas River basin is identified as the main factor contributing to variations in SSC. However, natural factors such as wind can influence the spatial distribution of SSC within the river. Additionally, human activities like channel dredging and the creation of artificial structures can also affect the spatial patterns of SSC.

Currently, the dredging of the El Palmar islet is being carried out to improve navigation conditions by deepening the river channel. This procedure is essential to facilitate the safe movement of larger vessels, which is crucial for commercial activities and maritime transport. In addition to optimizing navigation, dredging contributes to flood mitigation by increasing the river's capacity to handle large volumes of water, thus reducing the risk of overflows. Likewise, it plays an essential role in the maintenance of port infrastructure, guaranteeing the operation and efficiency of ports and docks. On the other hand, this process contributes to improving water quality by eliminating contaminated sediments, which offers benefits to both the aquatic ecosystems and human health.

DATA AVAILABILITY STATEMENT

The dataset is available upon request from the authors.

REFERENCES

- [1] *The United Nations World Water Development Report 2023: partnerships and cooperation for water*. Paris, France: UNESCO, 2023.
- [2] E. Vargas-Amelin and P. Pindado, "The challenge of climate change in Spain: Water resources, agriculture and land," *Journal of Hydrology*, vol. 518, pp. 243–249, Oct. 2014, <https://doi.org/10.1016/j.jhydrol.2013.11.035>.
- [3] S. Zhang, Y. Chen, X. Zhou, and Y. Zhang, "Climate and Human Impact Together Drive Changes in Ecosystem Multifunctionality in the Drylands of China," *Applied Soil Ecology*, vol. 193, Jan. 2024, Art. no. 105163, <https://doi.org/10.1016/j.apsoil.2023.105163>.
- [4] B. S. Takhellambam, P. Srivastava, J. Lamba, R. P. McGehee, H. Kumar, and D. Tian, "Projected Mid-Century Rainfall Erosivity Under Climate Change Over the Southeastern United States," *Science of The*

- Total Environment*, vol. 865, Mar. 2023, Art. no. 161119, <https://doi.org/10.1016/j.scitotenv.2022.161119>.
- [5] C. P. Harden, "Human impacts on headwater fluvial systems in the northern and central Andes," *Geomorphology*, vol. 79, no. 3, pp. 249–263, Sep. 2006, <https://doi.org/10.1016/j.geomorph.2006.06.021>.
- [6] E. I. López, "La gestión de los recursos hídricos en el Ecuador," *REGA - Revista de Gestão de Água da América Latina*, vol. 6, no. 2, pp. 33–48, Jul. 2009.
- [7] W. Buytaert, G. Wyseure, B. De Bièvre, and J. Deckers, "The effect of land-use changes on the hydrological behaviour of Histic Andosols in south Ecuador," *Hydrological Processes*, vol. 19, no. 20, pp. 3985–3997, 2005, <https://doi.org/10.1002/hyp.5867>.
- [8] W. Buytaert, V. Iñiguez, R. Celleri, B. De Bièvre, G. Wyseure, and J. Deckers, "Analysis of the Water Balance of Small Páramo Catchments in South Ecuador," in *Environmental Role of Wetlands in Headwaters*, Dordrecht, 2006, pp. 271–281, https://doi.org/10.1007/1-4020-4228-0_24.
- [9] F. Rossel, E. Cadier, and G. Gómez, "Las inundaciones en la zona costera ecuatoriana: causas, obras de protección existentes y previstas," *Bulletin de l'Institut Français d'Études Andines*, vol. 25, no. 3, pp. 399–420, 1996, <https://doi.org/10.3406/bifea.1996.1240>.
- [10] M. A. Hossain, T. Y. Gan, and A. B. M. Baki, "Assessing morphological changes of the Ganges River using satellite images," *Quaternary International*, vol. 304, pp. 142–155, Aug. 2013, <https://doi.org/10.1016/j.quaint.2013.03.028>.
- [11] G. R. Lesser, J. A. Roelvink, J. A. T. M. van Kester, and G. S. Stelling, "Development and validation of a three-dimensional morphological model," *Coastal Engineering*, vol. 51, no. 8, pp. 883–915, Oct. 2004, <https://doi.org/10.1016/j.coastaleng.2004.07.014>.
- [12] A. M. Teeter *et al.*, "Hydrodynamic and sediment transport modeling with emphasis on shallow-water, vegetated areas (lakes, reservoirs, estuaries and lagoons)," *Hydrobiologia*, vol. 444, no. 1, pp. 1–23, Feb. 2001, <https://doi.org/10.1023/A:1017524430610>.
- [13] T. H. Vu, D. V. Binh, H. N. Tran, M. A. Khan, D. D. Bui, and J. Stamm, "Quantifying Spatio-Temporal River Morphological Change and Its Consequences in the Vietnamese Mekong River Delta Using Remote Sensing and Geographical Information System Techniques," *Remote Sensing*, vol. 16, no. 4, Jan. 2024, Art. no. 707, <https://doi.org/10.3390/rs16040707>.
- [14] G. Alvarez-Mieles, K. Irvine, A. V. Griensven, M. Arias-Hidalgo, A. Torres, and A. E. Mynett, "Relationships between aquatic biotic communities and water quality in a tropical river-wetland system (Ecuador)," *Environmental Science & Policy*, vol. 34, pp. 115–127, Dec. 2013, <https://doi.org/10.1016/j.envsci.2013.01.011>.
- [15] Z. P. Simpson, R. W. McDowell, and L. M. Condrón, "Phosphorus attenuation in streams by water-column geochemistry and benthic sediment reactive iron," *Biogeosciences Discussions*, pp. 1–35, Oct. 2019, <https://doi.org/10.5194/bg-2019-400>.
- [16] J. E. Holguin-Gonzalez *et al.*, "Development and assessment of an integrated ecological modelling framework to assess the effect of investments in wastewater treatment on water quality," *Water Science and Technology*, vol. 70, no. 11, pp. 1798–1807, Jul. 2014, <https://doi.org/10.2166/wst.2014.316>.
- [17] H. E. Dregne, "Land Degradation in the Drylands," *Arid Land Research and Management*, vol. 16, no. 2, pp. 99–132, Jan. 2002, <https://doi.org/10.1080/153249802317304422>.
- [18] A. Goudie, *Encyclopedia of geomorphology*. London, New York: Routledge: International Association of Geomorphologists, 2004.
- [19] D. Pennock, *Soil Erosion: The Greatest Challenge for Sustainable Soil Management*, 1st ed. Rome, Italy: FAO, 2019.
- [20] C. B. Maniyar *et al.*, "Spatio-Temporal Dynamics of Total Suspended Sediments in the Belize Coastal Lagoon," *Remote Sensing*, vol. 15, no. 23, Jan. 2023, Art. no. 5625, <https://doi.org/10.3390/rs15235625>.
- [21] S. V. Balasubramanian *et al.*, "Robust algorithm for estimating total suspended solids (TSS) in inland and nearshore coastal waters," *Remote Sensing of Environment*, vol. 246, Sep. 2020, Art. no. 111768, <https://doi.org/10.1016/j.rse.2020.111768>.
- [22] L. Silveira Kupssinskü *et al.*, "A Method for Chlorophyll-a and Suspended Solids Prediction through Remote Sensing and Machine Learning," *Sensors*, vol. 20, no. 7, Jan. 2020, Art. no. 2125, <https://doi.org/10.3390/s20072125>.
- [23] A. Turner and G. E. Millward, "Suspended Particles: Their Role in Estuarine Biogeochemical Cycles," *Estuarine, Coastal and Shelf Science*, vol. 55, no. 6, pp. 857–883, Dec. 2002, <https://doi.org/10.1006/ecss.2002.1033>.
- [24] L. Fu, J. Deng, B. Zhu, Z. Li, and X. Liao, "AFOD: Two-stage object detection based on anchor-free remote sensing photos," *Open Computer Science*, vol. 14, no. 1, Jan. 2024, <https://doi.org/10.1515/comp-2023-0105>.
- [25] Z. Wang, H. Zhou, W. Ma, W. Fan, and J. Wang, "Land Surface Albedo Estimation and Cross Validation Based on GF-1 WFV Data," *Atmosphere*, vol. 13, no. 10, Oct. 2022, Art. no. 1651, <https://doi.org/10.3390/atmos13101651>.
- [26] N. Ambarita *et al.*, "Ecological water quality analysis of the Guayas river basin (Ecuador) based on macroinvertebrates indices," *Limnologia - Ecology and Management of Inland Waters*, vol. 57, pp. 27–59, Jan. 2016, <https://doi.org/10.1016/j.limno.2016.01.001>.
- [27] A. Deknock *et al.*, "Distribution of agricultural pesticides in the freshwater environment of the Guayas river basin (Ecuador)," *Science of The Total Environment*, vol. 646, pp. 996–1008, Jan. 2019, <https://doi.org/10.1016/j.scitotenv.2018.07.185>.
- [28] B. Bordel, R. Alcarria, J. Chung, and R. Kettimuthu, "Efficient and choreographed quality-of-service management in dense 6G verticals with high-speed mobility requirements," *Integrated Computer-Aided Engineering*, vol. 31, no. 2, pp. 173–195, Jan. 2024, <https://doi.org/10.3233/ICA-230722>.
- [29] C. Li and B. Xu, "Optimal scheduling of multiple Sun-synchronous orbit satellites refueling," *Advances in Space Research*, vol. 66, no. 2, pp. 345–358, Jul. 2020, <https://doi.org/10.1016/j.asr.2020.03.049>.
- [30] S. Kwon, H. Noh, I. W. Seo, and Y. S. Park, "Effects of spectral variability due to sediment and bottom characteristics on remote sensing for suspended sediment in shallow rivers," *Science of The Total Environment*, vol. 878, Jun. 2023, Art. no. 163125, <https://doi.org/10.1016/j.scitotenv.2023.163125>.
- [31] M. V. Japitana and M. E. C. Burce, "A Satellite-based Remote Sensing Technique for Surface Water Quality Estimation," *Engineering, Technology & Applied Science Research*, vol. 9, no. 2, pp. 3965–3970, Apr. 2019, <https://doi.org/10.48084/etasr.2664>.
- [32] F. Wang, B. Zhou, X. Liu, G. Zhou, and K. Zhao, "Remote-sensing inversion model of surface water suspended sediment concentration based on in situ measured spectrum in Hangzhou Bay, China," *Environmental Earth Sciences*, vol. 67, no. 6, pp. 1669–1677, Nov. 2012, <https://doi.org/10.1007/s12665-012-1608-0>.
- [33] X. Zhang, W. Qiao, Y. Lu, J. Huang, and Y. Xiao, "Quantitative Analysis of the Influence of the Xiaolangdi Reservoir on Water and Sediment in the Middle and Lower Reaches of the Yellow River," *International Journal of Environmental Research and Public Health*, vol. 20, no. 5, Jan. 2023, Art. no. 4351, <https://doi.org/10.3390/ijerph20054351>.